

Combined bending-tension/compression deformation of micro-bars accounting for strain-driven long-range interactions

N. ZHANG¹⁾, J. W. YAN²⁾, C. LI^{1,*}, J. X. ZHOU³⁾

¹⁾*Department of Vehicle Engineering, School of Rail Transportation, Soochow University, Suzhou 215131, Jiangsu, China*
**e-mail: licheng@suda.edu.cn*

²⁾*Key Laboratory of Product Packaging and Logistics of Guangdong Higher Education Institutes, Jinan University, Zhuhai, Guangdong, China*

³⁾*State Key Laboratory of Mechanics and Control of Mechanical Structures and College of Aerospace Engineering, Nanjing University of Aeronautics and Astronautics, Nanjing, 210016, China*

THE PAPER AIMS TO INVESTIGATE combined bending-tension/compression deformation of a micro-bar. The *strain-driven* nonlocal differential model which involves information about long-range interactions between atoms is used to develop the mechanical model and theoretical formulations. Subsequently, effects of internal long-range scale parameter, length of micro-bar, external loads and bending rigidity on combined deformation are shown and discussed. In particular, the upper bound of internal long-range scale parameter and the buckling load are achieved during bending-compression analyses. It is demonstrated that the existence of internal scale parameter or axial tensile load decreases combined deformation. The deflection at the midpoint reduces with increasing bending rigidity, while it rises with increasing length of the micro-bar. Additionally, an effect of the acting position of transverse load on combined deformation is discussed and deflection at the symmetry point of transverse acting position is achieved. When the long-range interaction is taken into consideration, the equivalent stiffness of the micro-bar subjected to combined bending-tension is stiffer than that predicted by classical mechanics, and it validates the existing nonlocal hardening model. The combined bending-compression of the micro-bar reveals that the deflection may increase or decrease with an increase in the long-range scale or structural length, which verifies both the nonlocal softening and hardening models.

Key words: micro-bar, combined deformation, internal scale, long-range interaction, bending-tension, bending-compression.

Copyright © 2019 by IPPT PAN, Warszawa

1. Introduction

THE MECHANICAL BEHAVIORS OF MATERIALS AND STRUCTURES at micro/nano-scale are very different from those of classical counterparts at macro-scale due to the intrinsic size effect. It is important to study the unique properties of micro-materials/structures and thus forms a new subject of micro-mechanics.

The micro-mechanics is attracting more and more interest and there is an increasing number of publications on statics and dynamics or thermal dynamics of micro-materials/structures including micro-tubes, micro-bars, micro-beams, micro-plates and so on [1–4]. A micro-bar-like structure is one of the most familiar components in micro-electro-mechanical-systems (MEMS) and the structure is often subjected to the combined bending-tension/compression deformation at work in micro-engineering. Hence it is necessary to understand and control the mechanical properties of the combined deformation of micro-bars and the related studies have been an indispensable part of micro/nano-mechanics and micro/nano-technology during past years. In combined deformation, the bending deformation dominates remarkably due to the combined effects of axial and transverse loads. Under such a condition, the axial load plays a significant role and cannot be omitted.

For the traditional bar with a macro-length scale, the classical mechanics of materials is useful to characterize its mechanical properties. However, the classical mechanics of materials fails to describe new properties of the micro-bar because the internal characteristic length scale is almost at the same order of magnitude as the external length scale and hence the long-range interactions should be taken into consideration. Fortunately, the nonlocal theory initiated by ERINGEN and EDELEN [5] can be used to measure the long-range interactions in stress-strain relation. Later on ERINGEN [6] rewrote the theory using a differential constitutive relation in order to avoid basic mathematical difficulties. In nonlocal theory, the micro-material/structure is treated as a continuum and the stress at a reference point in a continuum is assumed to be a function related to not only the strain at that point, but also depends on the strains at all other points in the continuum. Such a definition and concept are in accordance with the atomic theory of lattice dynamics and phonon dispersion. In fact, the nonlocal theory is one of the general continuum mechanics theories, and it is in the framework of viewpoint that the interaction force between atoms belongs to the long-range pattern. During the development of the nonlocal theory, two types of nonlocal constitution have been formed, namely the strain-driven nonlocal constitution (cf. [7–23]) and the stress-driven nonlocal constitution (cf. [24–32]). Firstly, the Eringen's nonlocal elasticity formulated by ERINGEN [6] considers an integral convolution whose input and output fields are the elastic strain and stress, respectively. The kernel of the convolution was chosen to be the fundamental solution of a differential problem in Euclidean space, under the condition of vanishing at infinity. In this context, the integral law can be conveniently substituted with the equivalent differential problem. This is the strain-driven nonlocal constitution [6]. The strain-driven constitution was resorted to in applications to continuous bounded micro/nano-structures by PEDDIESON *et al.* [7]. Subsequently, the application of strain-driven nonlo-

cal constitution was extended to two-dimensional nano-structures by ANSARI *et al.* [9] in which the free vibration of single-layered graphene was investigated using a nonlocal plate model. XU *et al.* [13] studied the mechanical behaviors of cantilever nano-beams using the strain-driven nonlocal constitution and observed the nano-structural softening phenomena. However, LIM *et al.* [18] concluded some new predictions on stiffness strengthening effects for buckling instability of nano-tubes. HUANG [21] presented the longitudinal free vibration of nano-rods and revealed the nonlocal scale effect by considering the internal long-range interactions. On the other hand, the stress-driven nonlocal constitution has been proposed by ROMANO and BARRETTA [24] recently. Unlike the strain-driven nonlocal constitution, the roles of stress and elastic strain fields are swapped in the stress-driven nonlocal constitution. The constitutive boundary conditions were derived from the stress-driven nonlocal relation. Under the condition of a special kernel function, the equivalence between stress-driven (integral) and strain-driven (differential) constitutions was proven by ROMANO and BARRETTA [24] successfully. Although the stress-driven model was developed only one year ago, nano-structural applications of the stress-driven constitution especially the nano-beams have been extensively carried out. For example, ROMANO *et al.* [25] developed the nonlocal integral model for elastic nano-beams based on the stress-driven constitution. Some enlightening comparisons and discussion between strain-driven, stress-driven and local/nonlocal hybrid models were presented from theoretical and computational perspectives. Combining the nonlocal strain gradient theory proposed by LIM *et al.* [32], BARRETTA *et al.* [27] examined the vibration of functionally graded Timoshenko nano-beams using the stress-driven constitution. Furthermore, BARRETTA and DE SCIARRA [31] established the nonlocal strain gradient constitutive boundary conditions for the first time. It was shown that the constitutive boundary conditions obey the nonlocal equilibrium relation. Therefore, it provides a perfect complement to the nonlocal strain gradient theory [32]. In short, the stress-driven model improves the nonlocal theory and it is valid to investigate the mechanical properties of nano-structures.

From the aforementioned analyses, it is shown that both the strain-driven and stress-driven nonlocal constitutions have been investigated and applied in micro-mechanics to reveal the long-range scale effect in a great number of research articles. From vast literature, people were surprised to find two opposite nonlocal elastic models based on the strain-driven nonlocal constitutions. One of them concludes the equivalent micro-structural stiffness predicted by the nonlocal theory is lower than that by the classical continuum theory, while the other achieves a reversed summary. Consequently, the two models were named as the nonlocal softening model [7–15] and nonlocal hardening model [16–23], respectively. The nonlocal long-range effect is characterized by the dimensionless scale

parameter $\tau = e_0 a/L$ where the product $e_0 a$ is a nonlocal parameter representing the internal long-range scale and L is the corresponding external characteristic length scale. Afterwards, both nonlocal models were verified [33–36] and they were proved to be surface-property-related phenomena in strain-driven nonlocal mechanics. The attractive and repulsive interactions among atoms on the surface result in the nonlocal softening and hardening models, respectively. In fact, the two reversed strain-driven based models can also be explained by the stress-driven model. This is because the structural rigidity predicted in a stress-driven model is stiffer [24], which is consistent with the new prediction that the stiffness is strengthened with increasing the nonlocal parameter [16–23].

In the present work, the strain-driven nonlocal elastic model is employed to describe the combined bending-tension/compression deformation of micro-bars. Regarding the micro-bar, it usually acts as a basic element in MEMS including micro-sensor, micro-oscillator and drug micro-screening, where the element frequently generates the combined bending-tension/compression deformation. For this purpose, the nonlocal long-range differential constitution for the bending moment of bars at micro-scale is derived and applied to the bending formulation in a classical equilibrium equation. Subsequently, the deflection at the midpoint and deflection at the symmetry point of acting point of transverse load are respectively obtained by solving the strain-driven nonlocal differential equation. The effects of the internal long-range scale, length, bending rigidity, axial and transverse loads, and acting point of transverse load on combined deformation are exhibited in detail. The upper bound of the internal long-range scale parameter and the buckling load are determined accordingly. The strain-driven nonlocal results are compared with the corresponding classical solutions in order to reveal the long-range scale effect. In particular, both the nonlocal softening and hardening models were validated again from the observations of the present combined bending-tension/compression deformation of micro-bars. The work can provide useful reference for designing a micro-bar since it is a commonly seen element in MEMS.

2. Combined bending-tension deformation

The nonlocal theory was firstly introduced by ERINGEN and EDELEN [5] using the vehicles of global balance laws and the second law of thermodynamics. After the derivation of the nonlocal theory using an integro-partial-differential equation, ERINGEN [6] proposed a nonlocal differential constitutive relation that connects the nonlocal stress with the classical counterpart clearly, which is called the strain-driven nonlocal model. The strain-driven nonlocal differential constitution provides a great deal of simplicity over the integro-partial-differential relation. The analytical solutions of screw dislocation and surface waves were easily ob-

tained via the strain-driven differential constitutive relation by ERINGEN [6]. The strain-driven nonlocal model includes a differential relation with an explicit scale parameter, and that scale parameter plays a remarkable role in predicting the distinctive performances of micro/nano-structures. As a result, it has been applied extensively to micro/nano-mechanics during past decades. The well-known strain-driven nonlocal differential equation incorporating a small scale effect and long-range interactions between atoms/molecules is expressed by [6]

$$(2.1) \quad \boldsymbol{\sigma}_{\text{nonl}} - (e_0 a)^2 \nabla^2 \boldsymbol{\sigma}_{\text{nonl}} = \boldsymbol{\sigma}_{\text{cla}} = \mathbf{C} : \boldsymbol{\varepsilon}$$

where $\boldsymbol{\sigma}_{\text{nonl}}$ and $\boldsymbol{\sigma}_{\text{cla}}$ are the nonlocal and classical stress tensors, respectively; $\boldsymbol{\varepsilon}$ is the strain tensor; \mathbf{C} is the elastic tensor and $e_0 a$ is the nonlocal scale parameter denoting the long-range interactions at micro/nano-scale; ∇^2 is the Laplacian operator. In fact, e_0 is the nonlocal material constant depending on different material properties, while a is the internal characteristic length scale such as lattice parameter, granular distance and so on [6]. The combination of $e_0 a$ was introduced to the nonlocal theory to characterize the inter-atomic long-range forces, which should be taken into account when the external characteristic length scale (e.g. wavelength, crack size) is almost at the same level as the internal characteristic length scale. It is noticed that the strain-driven nonlocal model can also be treated as a gradient type of a nonlocal model. This is because the solution to Eq. (2.1) can be expressed as a summation of classical strain and the strain gradients, as [22]

$$(2.2) \quad \boldsymbol{\sigma} = \mathbf{C} : \sum_{m=0}^{\infty} (e_0 a)^{2m} \nabla^{2m} \boldsymbol{\varepsilon}.$$

On the other hand, for a micro-bar with a length l bearing an axial tensile or compressive load P and transverse load Q , we assume the distance from the point of transverse load Q to the right end of micro-bar is d , as illustrated in Fig. 1. Because the deformation is small, we can suppose the axial load is still horizontal after deformation in Fig. 1.

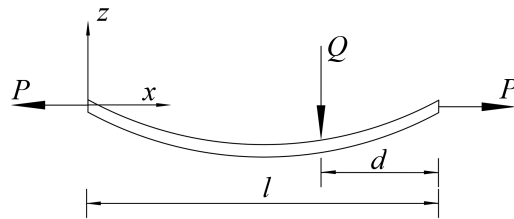


FIG. 1. Sketch of a micro-bar subjected to combined bending-tension deformation.

First we consider the combined bending-tension deformation. Denoting deflection at the position x in the axial direction coordinate is w , one can obtain the bending moments for both segments of the micro-bar, shown as

$$(2.3) \quad M = \frac{Qd}{l}x + Pw_1$$

when $0 \leq x \leq l - d$;

$$(2.4) \quad M = \frac{Q(l-d)(l-x)}{l} + Pw_2$$

when $l - d \leq x \leq l$.

In the present article, the strain-driven nonlocal theory is utilized to capture the long-range interactions occurring in combined bending-tension/compression deformation of micro-bar. Consequently, the one-dimensional simplified form of nonlocal differential Eq. (2.1) is required. After that, we further consider the relation between bending moment and bending stress defined in classical mechanics of materials $M = -\int_A z\sigma dA$ in which z is the thickness coordinate and A is the area of the cross section. Note that the minus sign in bending moment-stress relation is caused by the directions of the transverse load and z -axis. The deformation is shown in Fig. 1 according to the direction of the transverse load. In such a situation of deformation shape, the directions of stress σ and thickness axis (z -coordinate) are opposite, that is, the stress σ is negative and the z -coordinate is positive above the neutral layer of micro-bars, while the stress σ is positive and the z -coordinate is negative below the neutral layer. Hence, one can arrive at the expression of the nonlocal bending moment versus bending deflection, as

$$(2.5) \quad M - (e_0a)^2 \frac{d^2M}{dx^2} = EI \frac{d^2w}{dx^2}$$

where $I = \int_A z^2 dA$ is the area moment of inertia, E is Young's modulus and $\sigma_{\text{cla}} = E\varepsilon_{\text{cla}} = -Ez \frac{d^2w}{dx^2}$ is adopted. Obviously, if e_0a is zero in Eq. (2.5), or the intrinsic length scale representing the long-range interactions is negligible compared to external characteristic scale (e.g. for a bulk material or structure with macro-scale), the bending moment-deflection relation (2.5) becomes the counterpart of classical continuum mechanics.

Inserting Eqs. (2.3) and (2.4) into (2.5) yields, respectively

$$(2.6) \quad [EI + (e_0a)^2P] \frac{d^2w_1}{dx^2} - Pw_1 - \frac{Qd}{l}x = 0,$$

$$(2.7) \quad [EI + (e_0a)^2P] \frac{d^2w_2}{dx^2} - Pw_2 - \frac{Q(l-d)(l-x)}{l} = 0.$$

The general solutions to Eqs. (2.6) and (2.7) can be written respectively as

$$(2.8) \quad w_1 = A \exp\left[\sqrt{\frac{P}{EI + (e_0a)^2P}}x\right] + B \exp\left[-\sqrt{\frac{P}{EI + (e_0a)^2P}}x\right] - \frac{Qd}{Pl}x,$$

$$(2.9) \quad w_2 = C \exp\left[\sqrt{\frac{P}{EI + (e_0a)^2P}}x\right] + D \exp\left[-\sqrt{\frac{P}{EI + (e_0a)^2P}}x\right] - \frac{Q(l-d)(l-x)}{Pl}$$

where A , B , C and D are undetermined coefficients. In static analysis, only the boundary conditions are needed for finding these coefficients. Taking the fixed-fixed ends as an example, the boundary constraints require the deflections of both ends are zero, or $w_1 = 0$ at $x = 0$; $w_2 = 0$ at $x = l$. In addition to the boundary conditions, the continuity condition should also be considered as $w_1 = w_2$ and $dw_1/dx = dw_2/dx$ at $x = l - d$, which means the deflection and rotation angle of the left segment of micro-bar must coincide with those of the right segment. Based on the boundary and continuity conditions one arrives at

$$(2.10) \quad \begin{aligned} A &= \frac{e^{-m(l-d)}(e^{2ml} - e^{2m(l-d)})\xi}{2m(e^{2ml} - 1)}, & B &= -\frac{e^{-m(l-d)}(e^{2ml} - e^{2m(l-d)})\xi}{2m(e^{2ml} - 1)}, \\ C &= -\frac{e^{-m(l-d)}(e^{2m(l-d)} - 1)\xi}{2m(e^{2ml} - 1)}, & D &= \frac{e^{m(l+d)}(e^{2m(l-d)} - 1)\xi}{2m(e^{2ml} - 1)} \end{aligned}$$

where $m = \sqrt{P/(EI + (e_0a)^2P)}$ and a dimensionless factor $\xi = Q/P$ is defined. Consequently, the nonlocal bending deflections accounting for the long-range interactions are thus determined, respectively:

$$(2.11) \quad w_1 = \frac{e^{-m(l-d)}(e^{2ml} - e^{2m(l-d)})\xi}{2m(e^{2ml} - 1)}e^{mx} - \frac{e^{-m(l-d)}(e^{2ml} - e^{2m(l-d)})\xi}{2m(e^{2ml} - 1)}e^{-mx} - \frac{\xi d}{l}x,$$

$$(2.12) \quad w_2 = -\frac{e^{-m(l-d)}(e^{2m(l-d)} - 1)\xi}{2m(e^{2ml} - 1)}e^{mx} + \frac{e^{m(l+d)}(e^{2m(l-d)} - 1)\xi}{2m(e^{2ml} - 1)}e^{-mx} - \frac{\xi(l-d)(l-x)}{l}.$$

In fact, we can check the solutions expressed in Eqs. (2.11) and (2.12) via a simple way. Suppose $d=0$ which means the transverse load acts at the right fixed end, we can predict the deflection should be zero. It can be confirmed

from Eq. (2.11) since its interval is $0 \leq x \leq l - d$. On the other hand, suppose $d = l$ which means the transverse load acts at the left fixed end, we can predict the deflection should also be zero. It can be confirmed from Eq. (2.12) since its interval is $l - d \leq x \leq l$. Hence, the correctness of solutions (2.11) and (2.12) is achieved. Furthermore, the deflection at the midpoint of the micro-bars is

$$(2.13) \quad w_{\text{midpoint}} = \frac{e^{-m(l-d)}(e^{2ml} - e^{2m(l-d)})\xi}{2m(e^{2ml} - 1)} e^{ml/2} - \frac{e^{-m(l-d)}(e^{2ml} - e^{2m(l-d)})\xi}{2m(e^{2ml} - 1)} e^{-ml/2} - \frac{\xi d}{2}$$

when $l \geq 2d$,

$$(2.14) \quad w_{\text{midpoint}} = -\frac{e^{-m(l-d)}(e^{2m(l-d)} - 1)\xi}{2m(e^{2ml} - 1)} e^{ml/2} + \frac{e^{m(l+d)}(e^{2m(l-d)} - 1)\xi}{2m(e^{2ml} - 1)} e^{-ml/2} - \frac{\xi(l-d)}{2}$$

when $l \leq 2d$.

In particular, when the action position of the transverse load Q is at the middle of the micro-bar, i.e. $d = l/2$, the deflection at the midpoint of the micro-bar can be reduced via either Eq. (2.13) or (2.14) as

$$(2.15) \quad w_{\text{midpoint}} = \frac{(e^{ml} - 1)^2 \xi}{2m(e^{2ml} - 1)} - \frac{\xi l}{4}.$$

It is obvious that the deflection at the midpoint is proportional to the transverse load Q , which is the simplest correlation among various variables in this study. It is easy to understand from the basic viewpoint of classical mechanics of materials and is unnecessary to discuss. However, it is not inversely proportional to the axial tensile load P because not only the expression of ξ but also m contains P . In order to illustrate effects of the internal long-range scale parameter, length of the micro-bar, bending rigidity and external loads on the deflection at the midpoint, we present some numerical studies in Figs. 2–6 as follows. Note that the deflection is negative because of the directions of coordinate system and deformation shown in Fig. 1. It is observed that the deflection declines with increasing the internal long-range scale parameter from Fig. 2, hence the deflection containing long-range interactions is slightly lower than that predicted by classical continuum mechanics. For example, the nonlocal deflection reduces 3.44% or so when $e_0 a$ increases from 0 to 2 nm. Therefore, the equivalent stiffness of micro-structure is enhanced by the internal long-range scale effect, which is consistent with the prediction of the nonlocal hardening model [16–23] including

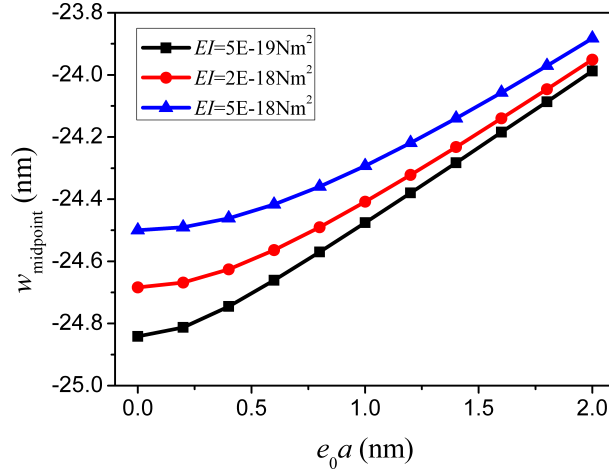


FIG. 2. The deflection at midpoint versus internal long-range scale parameter with different bending rigidity for combined bending-tension of micro-bars, where $P = Q = 5$ N, $l = 100$ nm.

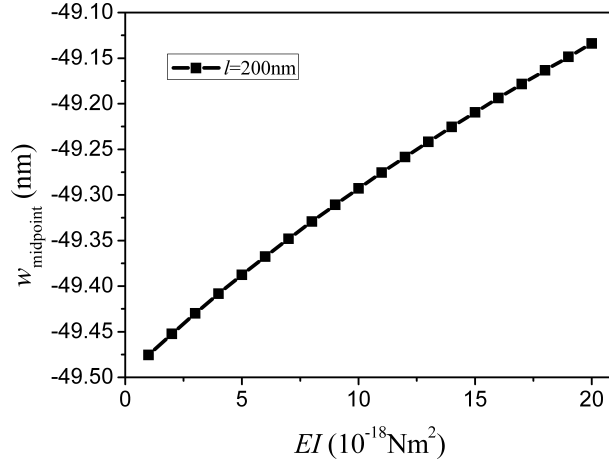


FIG. 3. The deflection at midpoint versus bending rigidity for combined bending-tension of micro-bars, where $P = Q = 10$ N. $e_0a = 1$ nm.

the previous work on long-range interactions [20, 21], that is, smaller is stiffer. So the validity of the present study is confirmed. On the other hand, the nonlocal deflection decreases with an increase in bending rigidity from Fig. 3, which resembles the classical mechanics of materials. A larger tensile load results in a smaller deflection from Fig. 4, and this is because the tensile load enhances the micro-structural stiffness. The deflection at the midpoint grows with increas-

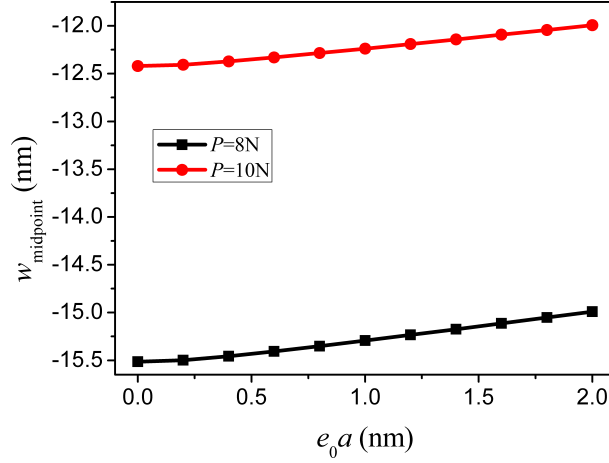


FIG. 4. The deflection at midpoint versus internal long-range scale parameter with different tensile load for combined bending-tension of micro-bars, where $Q = 5\text{ N}$, $l = 100\text{ nm}$, $EI = 10^{-18}\text{ Nm}^2$.

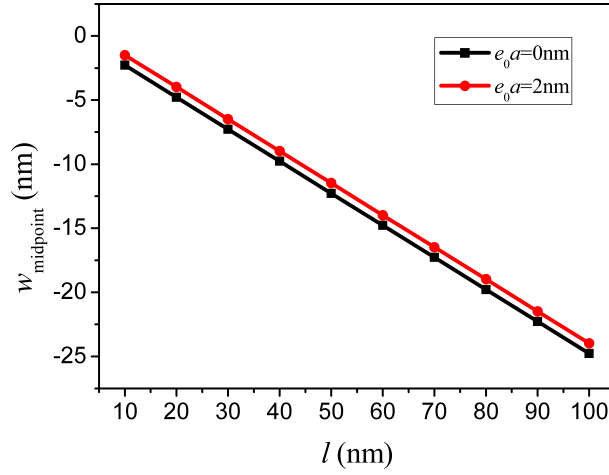


FIG. 5. The deflection at midpoint versus length with different internal long-range scale parameter for combined bending-tension of micro-bars, where $P = Q = 5\text{ N}$, $EI = 10^{-18}\text{ Nm}^2$.

ing the length of micro-bars from Fig. 5, and this is because a longer micro-bar means a higher flexibility. A nonlinear relationship between the deflection at the midpoint and a tensile load is shown in Fig. 6. Additionally, with the tensile load rising, a couple effect of bending rigidity and a tensile load is observed in Fig. 6. For a sufficient large tensile load, the results obtained from different bending rigidity are very close to each other, which implies the larger tensile load domi-

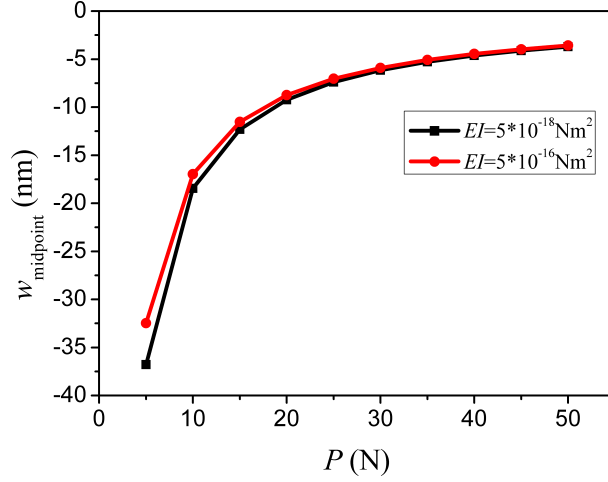


FIG. 6. The deflection at midpoint versus axial tensile load with different bending rigidity for combined bending-tension of micro-bars, where $Q = 5 \text{ N}$, $e_0 a = 1 \text{ nm}$, $l = 150 \text{ nm}$.

notes the stiffness otherwise the stiffness is influenced predominantly by bending rigidity if the tensile load becomes smaller.

3. Combined bending-compression deformation

Next we consider the combined bending-compression deformation via the strain-driven nonlocal constitutive relation. According to the opposite directions of tensile and compressive loads, the nonlocal deflection equations can be written directly by replacing P by $-P$ in Eqs. (2.6) and (2.7), but one cannot do the same actions on Eqs. (2.8) and (2.9) since the characteristic roots of the new differential equations are complex numbers (conjugated imaginary roots). The solutions for deflections of combined bending-compression deformation are resolved as

$$(3.1) \quad w_1 = A \cos \sqrt{\frac{P}{EI - (e_0 a)^2 P}} x + B \sin \sqrt{\frac{P}{EI - (e_0 a)^2 P}} x + \frac{\xi d}{l} x,$$

$$(3.2) \quad w_2 = C \cos \sqrt{\frac{P}{EI - (e_0 a)^2 P}} x + D \sin \sqrt{\frac{P}{EI - (e_0 a)^2 P}} x + \frac{\xi(l-d)(l-x)}{l}.$$

It is worth mentioning that the upper bound of internal long-range scale parameter can be determined for the combined bending-compression deformation

of micro-bars in order to ensure the existence of meaningful solutions, namely, the solutions for axial combined bending-compression deformation must include the terms with regard to nonlocal long-range interactions, or

$$(3.3) \quad (e_0 a)^{\text{up}} = \sqrt{\frac{EI}{P}}.$$

The relationship between the upper bound of the internal long-range scale parameter and the bending rigidity, the axial compressive load is shown in Fig. 7. It is implied that the upper bound of the internal long-range scale parameter changes significantly with the variations of bending rigidity and the axial compressive load. The upper bound decreases with an increase in the axial compressive load, while increases with an increase in bending rigidity. We can also conclude that the upper bound of internal long-range scale increases with increasing the axial tensile load. This can be explained as follows: (i) the axial tensile load is opposite to the axial compressive load; (ii) the existence of the axial tensile load contributes to strengthening the bending rigidity. Therefore, the axial compressive load reduces the bending rigidity. When increasing the bending rigidity or decreasing the axial compressive load, the upper bound of internal long-range scale increases. Of course, the upper bound may be different for different materials subjected to different loads or deformations. The result shown in Fig. 7 only suits for the special case of micro-bars with combined bending-compression deformation. Even so, it makes sense to determine the peak value of internal long-range scale because it is an unclear issue in vast literature.

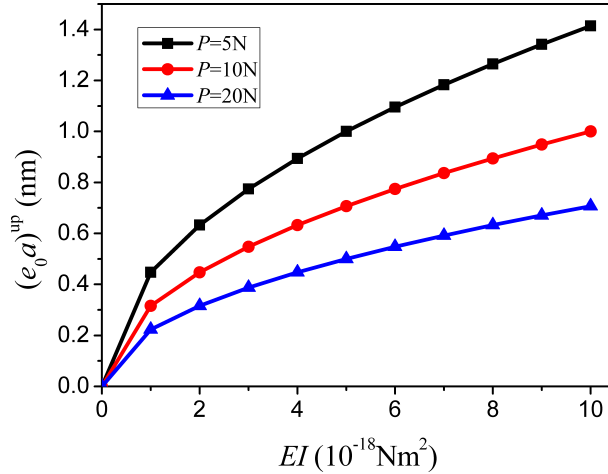


FIG. 7. Variations of the upper bound of internal long-range scale with respect to the bending rigidity and axial compressive load.

In addition to the upper bound of internal long-range scale, we can also investigate the buckling load from Eqs. (3.1) and (3.2) in such a bending-compression deformation. Because the expression under the radical sign in Eqs. (3.1) and (3.2) should be non-negative, the buckling load can be determined and the results are shown in Fig. 8. It is indicated that the buckling load increases with increasing the bending rigidity, which is easily understood since a larger bending rigidity means a stronger deformation resistant capability. Moreover, the buckling load decreases with an increase in the internal long-range scale parameter, which means the existence of a scale parameter makes the buckling load reduce. Hence, the buckling load predicted by the strain-driven nonlocal differential model is lower than that predicted by the classical continuum model. Such a conclusion is consistent with the nonlocal softening model since it deems the nano-structural stiffness is reduced.

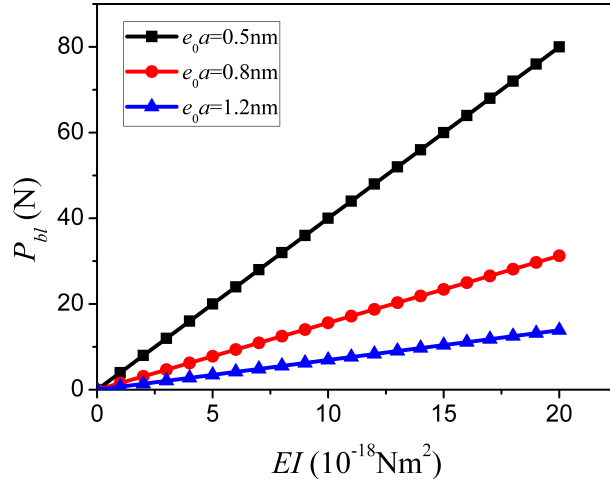


FIG. 8. Variations of the buckling load with respect to the bending rigidity and internal long-range scale parameter.

Still considering the boundary and continuity conditions for a doubly fixed micro-bar, that is $w_1 = 0$ at $x = 0$; $w_2 = 0$ at $x = l$; $w_1 = w_2$ and $dw_1/dx = dw_2/dx$ at $x = l - d$. The unknown coefficients can be determined from the general solutions shown in Eqs. (3.1) and (3.2) as well as the boundary and continuity conditions as:

$$(3.4) \quad \begin{aligned} A &= 0, & B &= \frac{\xi \{ \cot(nl) - \cot[n(l-d)] \} \sin[n(l-d)]}{n}, \\ C &= -\frac{\xi \sin[n(l-d)]}{n}, & D &= \frac{\xi \cot(nl) \sin[n(l-d)]}{n} \end{aligned}$$

where $n = \sqrt{P/(EI - (e_0a)^2P)}$. Therefore, we have

$$(3.5) \quad w_1 = \frac{\xi\{\cot(nl) - \cot[n(l-d)]\} \sin[n(l-d)]}{n} \sin nx + \frac{\xi d}{l} x,$$

$$(3.6) \quad w_2 = -\frac{\xi \sin[n(l-d)]}{n} \cos nx + \frac{\xi \cot(nl) \sin[n(l-d)]}{n} \sin nx \\ + \frac{\xi(l-d)(l-x)}{l}.$$

The correctness of solutions (3.5) and (3.6) can also be testified using two special cases. One is $d = 0$ or the transverse load acts at the right fixed end, we should use solution (3.5) to prove that the deflection is zero, which accords with the special force status. Another is $d = l$ or the transverse load acts at the left fixed end, we should use solution (3.6) to prove that the deflection is indeed zero and that it is a reasonable result based on the force status. Considering the deflection at the action position of the transverse load Q , i.e. let $x = l - d$, and one can use either Eq. (3.5) or (3.6) due to the continuity of deflection, expressed as

$$(3.7) \quad w_Q = \frac{\xi\{\cot(nl) - \cot[n(l-d)]\} \sin^2[n(l-d)]}{n} + \frac{\xi d(l-d)}{l}.$$

The relation between the deflection at the action position of Q , the internal long-range scale parameter and the action position of Q (i.e. d from the right end of the micro-bar) is plotted in Fig. 9. Unlike the combined bending-tension deformation, the deflection of combined bending-compression reveals a remarkable feature of jumping up and down. It is noticed that the classical solution is recovered with $e_0a = 0$ from the nonlocal theory, i.e. the left-most value in Fig. 9 represents the classical solution for each case ($d = l/4$, $d = l/3$ and $d = l/2$). Consequently, the nonlocal deflection containing long-range interactions with $e_0a \neq 0$ may be higher or lower than the classical deflection with $e_0a = 0$. The ratio of the nonlocal deflection to classical deflection being greater than one corresponds to the nonlocal softening model, while the ratio of the nonlocal to classical deflections being less than one corresponds to the nonlocal hardening model. As a result, although the non-monotonic performances of deflection w_Q with respect to e_0a is mainly caused by the particularity of trigonometric functions in solution (3.7) mathematically, Fig. 9 validates both the nonlocal softening and hardening models physically, which is consistent with the previous work [33–36]. In addition, the most significant effect of the action position on the deflection appears at $e_0a = 0.35$, namely the maximum differences of the deflection for the different action position d occur when $e_0a = 0.35$, and the deflections at this point are -4.78 nm, 0.019 nm and -10.06 nm for $d = l/4$, $d = l/3$ and $d = l/2$, respectively. Considering the structural symmetry, we only

examine three cases for $d = l/4$, $d = l/3$ and $d = l/2$. That is, we only choose three different positions on the right half segment of the micro-bar. It is shown that when the transverse load acts on the position of $d = l/3$, the amplitude of change for the deflection at the action position is relatively non-intense, while when the transverse load acts on the positions of $d = l/4$ and $d = l/2$, the deflection at the action position changes more sharply.

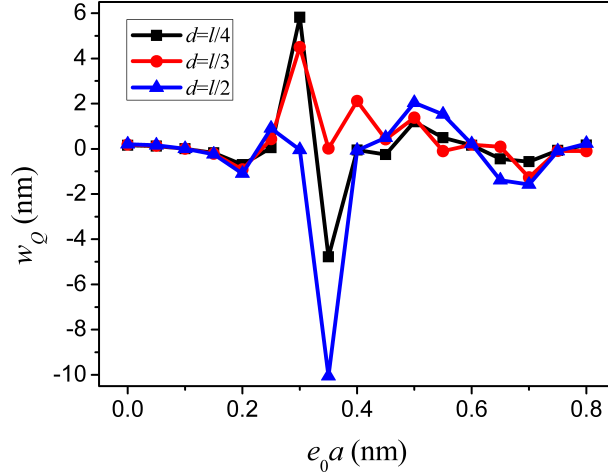


FIG. 9. Effects of the internal long-range scale and action position of transverse load on deflection at action position, where $P = Q = 10$ N, $EI = 10^{-17}$ Nm², $l = 150$ nm.

As the last case study, we calculate that when the transverse load acts at $d = l/4$, the deflection at its symmetry point (the symmetry point of the acting point of the transverse load, i.e. $x = l/4$ on the micro-bar). Because the symmetry point is on the left of the transverse load, we should use Eq. (3.5) to calculate the deflection. Substituting $d = l/4$ and $x = l/4$ into Eq. (3.5) yields

$$(3.8) \quad w_{l/4} = \frac{\xi}{n} \left[\cot(nl) - \cot \frac{3nl}{4} \right] \sin \frac{nl}{4} \sin \frac{3nl}{4} + \frac{\xi l}{16}.$$

The relation between the deflection at the symmetry point and the length of the micro-bar is shown in Fig. 10. It is demonstrated that the deflection at the symmetry point increases overall with an increase in length l . It is equivalent to the conclusion summarized in Fig. 2, where the deflection decreases with an increase in the internal long-range scale $e_0 a$. This is because the internal long-range scale and the length of the micro-bar can represent the internal and external characteristic scales, respectively. In most previous studies, one used a dimensionless nonlocal scale quantity $\tau = e_0 a/l$ in which the inverse relation between $e_0 a$ and l is seen. Moreover, the variations of deflection are not

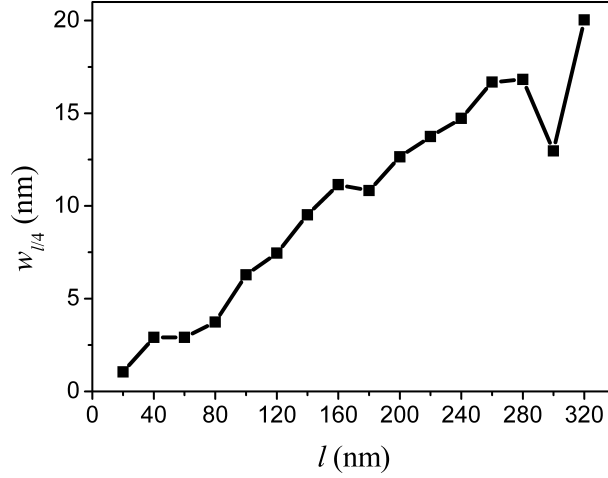


FIG. 10. Deflection at the symmetry point of acting point of transverse load when $d = l/4$, where $P = Q = 2$ N, $EI = 10^{-18}$ Nm², $e_0a = 0.5$ nm.

always up with respect to length. At some particular values (e.g. $l = 300$ nm) the deflection may decrease. Such observation recalls the existence of nonlocal softening and hardening models again. Of course, the different performances between the combined bending-compression and bending-tension deformations are the combined bending-compression that contains the jumping phenomenon. The physical cause is that the micro-bar may become instable when the axial tension is replaced by axial compression. Consequently, the mechanical quantities may lose stability as shown in the numerical results.

4. Conclusions

The combined bending-tension and bending-compression deformations of micro-bars are examined by considering the nonlocal long-range interactions between atoms. The nonlocal bending moment relation is gained and the equilibrium equations of combined bending-tension/compression are developed, respectively. The analytical solutions for deflection are determined from the *strain-driven* nonlocal differential equations. It concludes that: (i) The deflection of combined bending-tension is influenced by the internal long-range scale, axial tensile load, bending rigidity and length of the micro-bar. It decreases with increasing the internal long-range scale, axial tensile load and bending rigidity, while increases with an increasing length of the micro-bar; (ii) The *linear* relation between the deflection and the transverse load, and the *nonlinear* relation between the deflection and the axial load are observed. The effect of both loads

cannot be neglected in combined deformations; (iii) The upper bound of internal long-range scale and the buckling load are obtained. The upper bound is related to the bending rigidity and the compressive load, while the other is related to the bending rigidity and internal long-range scale; (iv) The acting position of the transverse load has a significant influence on the deflection, and the deflection may *increase or decrease* with respect to the internal long-range scale or the length of the micro-bar for combined bending-compression. The major contribution of this paper is to reveal the mechanical properties of micro-bars subjected to combined deformations. In addition, both nonlocal softening and hardening performances are observed and validated.

Author contributions

N. Zhang and J.W. Yan contributed to the work equally and should be regarded as co-first authors.

Acknowledgements

This work was supported by Natural Science Foundation of China (No. 11702112), Open Project of State Key Laboratory of Mechanics and Control of Mechanical Structures (Nanjing University of Aeronautics and Astronautics) (The grant No. MCMS-0418G01). Also, the corresponding author is grateful for funding support from the Soochow Scholar Plan of Soochow University (No. R513300116). In particular, the constructive suggestions from anonymous reviewers are greatly appreciated.

References

1. L.F. WANG, H.Y. HU, *Flexural wave propagation in single-walled carbon nanotubes*, Physical Review B, **71**, 195412, 2005.
2. J. ZHAO, J.W. JIANG, L. WANG, W. GUO, T. RABCZUK, *Coarse-grained potentials of single-walled carbon nanotubes*, Journal of the Mechanics and Physics of Solids, **71**, 197–218, 2014.
3. E. SECCHI, S. MARBACH, A. NIGUES, D. STEIN, A. SIRIA, L. BOCQUET, *Massive radius-dependent flow slippage in carbon nanotubes*, Nature, **537**, 210–213, 2016.
4. J.N. JIANG, L.F. WANG, *Analytical solutions for thermal vibration of nanobeams with elastic boundary conditions*, Acta Mechanica Solida Sinica, **30**, 474–483, 2017.
5. A.C. ERINGEN, D.G.B. EDELEN, *On nonlocal elasticity*, International Journal of Engineering Science, **10**, 233–248, 1972.
6. A.C. ERINGEN, *On differential equations of nonlocal elasticity and solutions of screw dislocation and surface waves*, Journal of Applied Physics, **54**, 4703–4710, 1983.

7. J. PEDDIESON, G.R. BUCHANAN, R.P. MCNITT, *Application of nonlocal continuum models to nanotechnology*, International Journal of Engineering Science, **41**, 305–312, 2003.
8. Q. WANG, V.K. VARADAN, *Vibration of carbon nanotubes studied using nonlocal continuum mechanics*, Smart Materials and Structures, **15**, 659–666, 2006.
9. R. ANSARI, S. SAHMANI, B. ARASH, *Nonlocal plate model for free vibrations of single-layered graphene sheets*, Physics Letters A, **375**, 53–62, 2010.
10. F.M. DE SCIARRA, R. BARRETTA, *A new nonlocal bending model for Euler-Bernoulli nanobeams*, Mechanics Research Communications, **62**, 25–30, 2014.
11. L. LI, Y. HU, *Buckling analysis of size-dependent nonlinear beams based on a nonlocal strain gradient theory*, International Journal of Engineering Science, **97**, 84–94, 2015.
12. A. BAHRAMI, A. TEIMOURIAN, *Nonlocal scale effects on buckling, vibration and wave reflection in nanobeams via wave propagation approach*, Composite Structures, **134**, 1061–1075, 2015.
13. X.J. XU, Z.C. DENG, K. ZHANG, W. XU, *Observations of the softening phenomena in the nonlocal cantilever beams*, Composite Structures, **145**, 43–57, 2016.
14. Z. RAHIMI, G. REZAZADEH, W. SUMELKA, X.J. YANG, *A study of critical point instability of micro and nano beams under a distributed variable-pressure force in the framework of the inhomogeneous non-linear nonlocal theory*, Archives of Mechanics, **69**, 413–433, 2017.
15. H.B. LI, X. WANG, J.B. CHEN, *Nonlinear dynamic responses of triple-layered graphene sheets under moving particles and an external magnetic field*, International Journal of Mechanical Sciences, **136**, 413–423, 2018.
16. H.M. MA, X.L. GAO, J.N. REDDY, *A microstructure-dependent Timoshenko beam model based on a modified couple stress theory*, Journal of the Mechanics and Physics of Solids, **56**, 3379–3391, 2008.
17. C.W. LIM, *On the truth of nanoscale for nanobeams based on nonlocal elastic stress field theory: equilibrium, governing equation and static deflection*, Applied Mathematics and Mechanics, **31**, 37–54, 2010.
18. C.W. LIM, J.C. NIU, Y.M. YU, *Nonlocal stress theory for buckling instability of nanotubes: new predictions on stiffness strengthening effects of nanoscales*, Journal of Computational and Theoretical Nanoscience, **7**, 2104–2111, 2010.
19. C. LI, C.W. LIM, J.L. YU, *Dynamics and stability of transverse vibrations of nonlocal nanobeams with a variable axial load*, Smart Materials and Structures, **20**, 015023, 2011.
20. M. ZINGALES, *Wave propagation in 1D elastic solids in presence of long-range central interactions*, Journal of Sound and Vibration, **330**, 3973–3989, 2011.
21. Z. HUANG, *Nonlocal effects of longitudinal vibration in nanorod with internal long-range interactions*, International Journal of Solids and Structures, **49**, 2150–2154, 2012.
22. C. LI, *A nonlocal analytical approach for torsion of cylindrical nanostructures and the existence of higher-order stress and geometric boundaries*, Composite Structures, **118**, 607–621, 2014.
23. J.J. LIU, C. LI, C.J. YANG, J.P. SHEN, F. XIE, *Dynamical responses and stabilities of axially moving nanoscale beams with time-dependent velocity using a nonlocal stress gradient theory*, Journal of Vibration and Control, **23**, 3327–3344, 2017.

24. G. ROMANO, R. BARRETTA, *Nonlocal elasticity in nanobeams: the stress-driven integral model*, International Journal of Engineering Science, **115**, 14–27, 2017.
25. G. ROMANO, R. BARRETTA, M. DIACO, *On nonlocal integral models for elastic nanobeams*, International Journal of Mechanical Sciences, **131–132**, 490–499, 2017.
26. G. ROMANO, R. LUCIANO, R. BARRETTA, M. DIACO, *Nonlocal integral elasticity in nanostructures, mixtures, boundary effects and limit behaviours*, Continuum Mechanics and Thermodynamics, **30**, 641–655, 2018.
27. R. BARRETTA, S.A. FAGHIDIAN, R. LUCIANO, C.M. MEDAGLIA, R. PENNA, *Free vibrations of FG elastic Timoshenko nano-beams by strain gradient and stress-driven nonlocal models*, Composites Part B, **154**, 20–32, 2018.
28. R. BARRETTA, S. ALI FAGHIDIAN, R. LUCIANO, *Longitudinal vibrations of nano-rods by stress-driven integral elasticity*, Mechanics of Advanced Materials and Structures, DOI: 10.1080/15376494.2018.1432806, 2018.
29. R. BARRETTA, M. ČANADIJA, L. FEO, R. LUCIANO, F.M. DE SCIARRA, R. PENNA, *Exact solutions of inflected functionally graded nano-beams in integral elasticity*, Composites Part B, **142**, 273–286, 2018.
30. R. BARRETTA, M. DIACO, L. FEO, R. LUCIANO, F.M. DE SCIARRA, R. PENNA, *Stress-driven integral elastic theory for torsion of nano-beams*, Mechanics Research Communications, **87**, 35–41, 2018.
31. R. BARRETTA, F.M. DE SCIARRA, *Constitutive boundary conditions for nonlocal strain gradient elastic nano-beams*, International Journal of Engineering Science, **130**, 187–198, 2018.
32. C.W. LIM, G. ZHANG, J.N. REDDY, *A higher-order nonlocal elasticity and strain gradient theory and its applications in wave propagation*, Journal of the Mechanics and Physics of Solids, **78**, 298–313, 2015.
33. C. LI, *Torsional vibration of carbon nanotubes: comparison of two nonlocal models and a semi-continuum model*, International Journal of Mechanical Sciences, **82**, 25–31, 2014.
34. C. LI, S. LI, L.Q. YAO, Z.K. ZHU, *Nonlocal theoretical approaches and atomistic simulations for longitudinal free vibration of nanorods/nanotubes and verification of different nonlocal models*, Applied Mathematical Modelling, **39**, 4570–4585, 2015.
35. J.P. SHEN, C. LI, *A semi-continuum-based bending analysis for extreme-thin micro/nano-beams and new proposal for nonlocal differential constitution*, Composite Structures, **172**, 210–220, 2017.
36. C. LI, S.H. SUI, L. CHEN, L.Q. YAO, *Nonlocal elasticity approach for free longitudinal vibration of circular truncated nanocones and method of determining the range of nonlocal small scale*, Smart Structures and Systems, **21**, 279–286, 2018.

Received August 19, 2018; revised version December 6, 2018.

Published online February 27, 2019.